Limiting Cases and Approximate Solutions for Fixed-Bed Reactors with Periodic Flow Reversal

Ulrich Nieken, Grigorios Kolios, and Gerhart Eigenberger
Institut für Chemische Verfahrenstechnik, University of Stuttgart, D-70199 Stuttgart, Germany

Fixed-bed reactors with periodic flow reversal are used to carry out reactions with low exothermicity in an autothermal way. Contrary to conventional autothermal reactors, the preheating of the feed gas is accomplished by regenerative heat exchange between the gas and fixed bed. The feedback of heat and direct coupling of heat exchange and chemical reaction give rise to an unusual reactor behavior. This behavior can be understood through consideration of the limiting cases of very long and very short cycle periods. Both cases can be calculated easily with the methods presented. Especially for the case of rapid flow reversal, simple equations can be derived that allow for a good physical understanding of the process and for a preliminary reactor design. In this case, it is also possible to compute the unstable solution, which is a lower bound of the temperature profile necessary for reactor startup.

Introduction

Autothermal operation of fixed-bed reactors is applied for weakly to moderately exothermic reactions where the hot effluent is used to heat up the cold feed to the required ignition temperature of the reaction. Traditionally, heat exchange and chemical reaction are carried out in two different pieces of equipment: a countercurrent recuperative heat exchanger and an adiabatic packed-bed reactor. Recently, a new method of autothermal operation with periodic flow reversal has gained considerable interest. This method was developed and propagated by Boreskov and Matros and their group in Novosibirsk (Boreskov et al. 1979, 1982; Boreskov and Matros, 1983; Matros, 1986, 1989). In the former USSR, it is applied industrially for equilibrium-limited reactions (SO_3-, methanol-, ammonia-synthesis) as well as for gas purification (Matros et al., 1988, 1993). In western countries an increasing number of companies are using the same principle for the purification of air contaminated with low amounts of combustible gas or vapor (Eigenberger and Nieken, 1991).

As in standard autothermal operation, it is the objective to operate the reactor in the ignited steady state and to use the heat of the effluent to heat up the feed. Unlike in standard autothermal operation, the heat recovery is done by regeneration instead of recuperative heat exchange by using both ends of the fixed bed as regenerative heat exchangers. Figure 1 shows the basic mode of operation. After the fixed bed has been heated up to reaction temperature in a separate first step, the cold gas enters the packed bed from one side, is heated up to ignition temperature by the hot packing, and the reaction proceeds to the respective equilibrium conversion. Since the fixed bed in turn is cooled by the feed, the temperature front slowly moves in flow direction. After a certain portion of the fixed bed has been cooled down, the flow direction is reversed and a new front moves into the fixed bed from the opposite side, while the old front is pushed back. It usually takes a large number of flow reversals until the steady state of the periodic operation is established. In this steady state the two temperature fronts move back and forth in a completely symmetrical way (Figure 1b). Assuming adiabatic operation, the total heat generated is released with the exit gas, leading to a sawtoothlike exit temperature profile in time (Figure 1c).

In the case of total combustion reactions, the same mode of operation can be used both with catalytic packed beds and with inert packings. In the latter case the combustion takes place as a homogeneous gas-phase reaction, while the packing serves as a heat storage device.

Currently, the cyclic steady state of a fixed-bed reactor can only be obtained through dynamic simulation. This requires very time-consuming computations. It is the main objective of this article to present simplified models that can be used to calculate fast and accurate approximations of the steady-state

Correspondence concerning this article should be addressed to G. Eigenberger.
Present address of U. Nieken: BASF AG, Ludwigshafen, Germany.

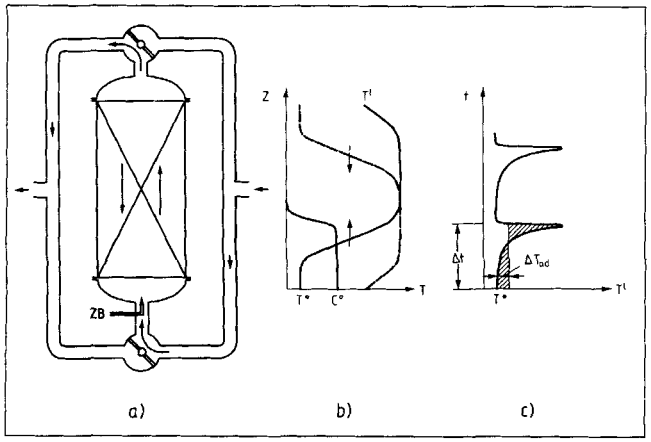

Figure 1. Reverse flow reactor.

(a) Reactor scheme; (b) temperature and concentration profiles in the oscillating steady state just before flow reversal; (c) outlet temperature vs. time.

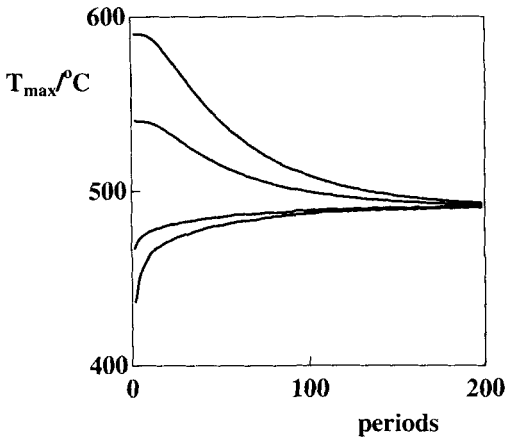

Figure 2. Maximum temperature vs. the number of flow reversals for different isothermal temperature profiles at $t = 0$.

Model parameters Table 1, set 1.

profiles. Additionally, these simplified models can help to gain a good understanding of the process and of the influence of all relevant process parameters. The approximate solutions will be compared to those of a conventional two-phase or a quasi-homogeneous model of the fixed-bed reactor under periodic operation. A detailed experimental investigation has been published elsewhere (Nieken et al., 1994).

The approximate solutions are based on the two limiting cases of the periodic operation. For very large switching periods the temperature profile approaches that of the stationary traveling reaction front. For very short switching periods the behavior of the reactor is similar to that of a countercurrent reactor.

The stationary traveling reaction front has been studied intensively by several authors during the last two decades. After the first detailed discussion by Wicke and Vortmeyer (1959), many investigations were published, mainly on the approximation of the maximum front temperature. Gilles (1974) used a quasi-homogeneous model and approximated the reactive heat-release curve by a Gaussian distribution. The parameters of the curve were adapted to the solution of the detailed model. Epple (1976) used the same model and a collocation technique for the determination of the parameters. This reduces the problem to the solution of a small system of nonlinear equations; however, the numerical solution requires a good initial guess. Pinjala et al. (1988) derived an equation for the approximation of the maximum temperature of the traveling wave, which is based on an approximation given by Kiselev and Matros (1980). We will use their approach in combination with the equivalence relation of Vortmeyer and Schäfer (1974) to derive a simple procedure for the calculation of the traveling reaction front.

An approximation to the temperature profile for short switching periods has first been presented by Matros (1989). The equations describing the so-called "sliding regime" are derived from the quasi-homogeneous model of the reactor with periodic flow reversal, and result in a stationary boundary value problem in space. Chumakova and Matros (1991) have published a study on the stability of the solutions of this model; however, the method used to calculate the solution is not given.

To avoid the time-consuming procedure of calculating the transition into the cyclic stationary regime, Bhatia (1991) used a perturbation analysis technique. The zero-order solution is symmetric, corresponding to the sliding regime. The first-order correction describes the parallel transposition of the profile in flow direction during one-half period. Another method to find the periodic stationary solution for the detailed two-phase model is presented by Gupta and Bhatia (1991). The system is transformed into a boundary-value problem in time. The advantage of this method is that no further simplifications are necessary for the numeric solution. Even then the computation of the Jacobian matrix is time-consuming, so only a rather small number of grid points is used. In addition, the neglection of axial conduction of heat in the catalyst phase is in many cases not justified.

To reduce the computational effort, and for the derivation of a simplified model, the equivalence relation between one- and two-phase models as proposed by Vortmeyer and Schäfer (1974) will be applied in the following, see Eq. 9. This transforms the two energy balances of the two-phase model into that of the quasi-homogeneous model. The two terms contributing to the effective axial heat conductivity are the axial heat conductivity of the solid and a term due to heat transfer between the gas and the solid. This relation has proved to be applicable both for packings and for honeycomb catalysts. In contrast, the equivalence relation derived by Chen and Luss (1989) is based on the assumption that there is no heat conduction in the solid phase; axial heat conduction due to vortices in the gas phase is considered instead.

Model Equations

For a detailed simulation of the process, a one-dimensional two-phase model that accounts for axial conduction and for heat and mass transfer between gas and packing is used. The model consists of the following equations:

Energy balance of the solid phase (temperature T^*):

$$(1-\epsilon)\cdot(\varrho c_p)s\cdot\frac{\partial T^*}{\partial t}=\lambda_s\cdot(1-\epsilon)\cdot\frac{\partial^2 T^*}{\partial z^2}+\alpha\cdot a_v\cdot(T-T^*)+a_v\cdot\sum_{i=1}^{I}(-\Delta h_{ri})\cdot r_i. \quad (1)$$

Energy balance of the gas phase (temperature T):

$$\epsilon\cdot\varrho_G\cdot c_{pG}\cdot\frac{\partial T}{\partial t}=\lambda_{G,ax}\cdot\epsilon\cdot\frac{\partial^2 T}{\partial z^2}-\frac{\dot m}{A}\cdot c_{pG}\cdot\frac{\partial T}{\partial z}-\alpha\cdot a_v\cdot(T-T^*). \quad (2)$$

Mass balance of the solid phase (concentration c_j^*):

$$\beta_j\cdot a_v\cdot(c_j-c_j^*)=-a_v\cdot\sum_{i=1}^{I}\nu ij\cdot r_i. \quad (3)$$

Mass balance of the gas phase (weight fraction g_j):

$$\epsilon\cdot\varrho_G\cdot\frac{\partial g_j}{\partial t}=D_{\text{eff}}\cdot\epsilon\cdot\frac{\partial^2 g_j}{\partial z^2}-\frac{\dot m}{A}\cdot\frac{\partial gi}{\partial z}-M_j\cdot\beta_i\cdot a_v\cdot(c_i-c_i^*). \quad (4)$$

These equations are subject to the conventional Danckwerts boundary conditions (Danckwerts, 1953) given below:

$$D_{\text{eff}}\cdot\epsilon\frac{\partial g_j}{\partial z}\bigg|_{z=0}=\frac{\dot m}{A}\cdot\left(g_j|_{z=0}-g_j^0\right).\qquad D_{\text{eff}}\cdot\epsilon\frac{\partial g_j}{\partial z}\bigg|_{z=L}=0. \quad (5)$$

$$\lambda_{G,ax}\cdot\epsilon\frac{\partial T}{\partial z}\bigg|_{z=0}=\frac{\dot m}{A}\cdot c_{pG}\cdot(T|_{z=0}-T^0).\ \lambda_{G,ax}\cdot\epsilon\frac{\partial T}{\partial z}\bigg|_{z=L}=0. \quad (6)$$

$$\frac{\partial T^*}{\partial z}\bigg|_{z=0}=0.\qquad \frac{\partial T^*}{\partial z}\bigg|_{z=L}=0. \quad (7)$$

The equivalence relation between one- and two-phased models as proposed by Vortmeyer and Schäfer (1974) transforms the two energy balances into that of the quasi-homogeneous model (the temperature T^* denotes the solid-phase temperature in case of a two-phase model and the averaged temperature in case of a quasi-homogeneous energy balance):

$$(1-\epsilon)\cdot(\varrho c_p)_S\cdot\frac{\partial T^*}{\partial t}=\lambda_{\text{eff}}\cdot\frac{\partial^2 T^*}{\partial z^2}-\frac{\dot m}{A}\cdot c_{pG}\cdot\frac{\partial T^*}{\partial z}+a_v\cdot\sum_{i=1}^{I}(-\Delta hr_i)\cdot r_i, \quad (8)$$

where the "effective" axial heat conductivity is given by

$$\lambda_{\text{eff}}=\lambda_S\cdot(1-\epsilon)+\left(\frac{\dot m\cdot c_{pG}}{A}\right)^2\cdot\frac{1}{\alpha\cdot a_v}. \quad (9)$$

Table 1. Model Parameters

	Parameter Set 1	Parameter Set 2	
	$d_h = 1.06$ mm	$d_h = 2$ mm	
D_{eff}	0.0001		kg/(m·s)
λ_G	0.0446		W/(m·K)
D	0.41		cm²/s
$(-\Delta h_r)$	2,040,236.0		kJ/kmol
$\dot m/A$	1.09		kg/(m²·s)
T^0	50		°C
Δt	60		s
$(1-\epsilon)\cdot(\varrho c_p)_S$	428.3		kJ/(m³·K)
c_{pG}	1.1		kJ/(kg·K)
ϵ	0.69		
λ_S	1.26		W/(m·K)
α	130.05	68.9	W/(m²·K)
β	0.1151	0.061	m/s
a_v	2,628.8	1,380.0	m²/m³

The physical properties of the bed refer to ceramic honeycomb catalysts with a hydraulic diameter of 1 mm (set 1) and 2 mm (set 2). The parameters α and β are determined for fully developed laminar flow in rectangular channels with $Nu = 3.091$, $Sh = 2.976$. The parameters of the gas are averages at $p = 1$ bar, $T = 350$°C.

Unless otherwise specified in the figure captions, the model parameters given in Table 1 have been used. In the simplified models, specified in the following, both gas-phase balances were considered in quasi-steady state, since the thermal time constant of the catalyst phase exceeds the time constant of the gas phase by three orders of magnitude. In addition, both dispersive terms in the gas-phase equations are neglected (that is, $\lambda_{\text{gas}} = D_{\text{eff}} = 0$) and only the heat conductivity λ_S in the solid phase was retained. The admissibility of these simplifications was proved through comparison with the full model results. Table 2 provides kinetic parameters.

Cyclic Steady State and Limiting Cases

Calculation of the cyclic steady state by integration of the model equations over a large number of flow reversals is very time-consuming. Figure 2 shows the transient of the maximum temperature in the reactor bed over the number of flow reversals for different initial temperature profiles. To obtain the final state, up to 200 flow reversals have to be computed. An integration procedure of high numerical accuracy is necessary because the steady-state solution is very sensitive to numerical errors (Nieken, 1993; Nowak et al., 1995).

Our key to finding simplified models for reversed flow reactors is based upon the relative invariance of both the shape and the maximum of the temperature front to variations of the switching period. Figure 3 shows the temperature profiles just before flow reversal for different cycle periods. Additionally, the limiting cases for very short switching periods ($\Delta t \rightarrow$

Table 2. Kinetic Parameters

$r_{\text{Propan}} = k^\infty\cdot e^{-E/R\cdot T^*}\cdot c^*$	kmol/m²$_{\text{Sur}}$·s
$c_j = g_j\cdot\frac{\varrho_G}{M_j},\quad \varrho_G=\frac{p\cdot M_L}{R\cdot T}$	
$k^\infty = 6{,}904.09$	m/s
$E = 69{,}247.13$	kJ/kmol

The kinetics are given for the total oxidation of traces of propane in air at atmospheric pressure on a platinum catalyst (Nieken, 1993).

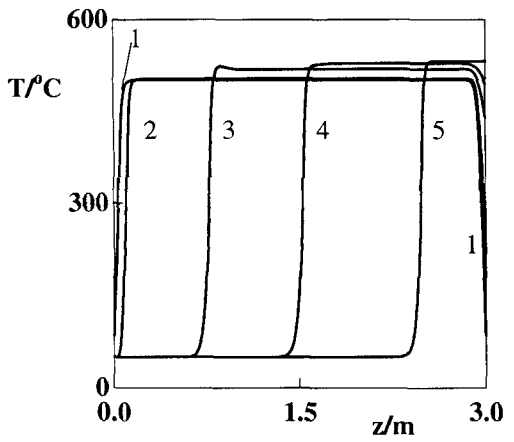

Figure 3. Temperature profiles as a function of the switching period.

(1) $\Delta t = 0$ s (countercurrent reactor); (2) $\Delta t = 30$ s; (3) $\Delta t = 300$ s; (4) $\Delta t = 600$ s; (5) $\Delta t = +\infty$ (stationary moving reaction front). (Length of reactor: 3 m, parameter set 1, Table 1.)

0, profile 1) and for very long periods in an infinitely long reactor ($\Delta t \rightarrow +\infty$, profile 5) are given. For very short switching periods, the reverse-flow reactor approaches the case of a countercurrent reactor. We will explain this in detail in the next section. Starting from profile 1, an increase of the cycle period leads to a shift of the profile, but the temperature gradient of the front and the maximum temperature are only slightly affected. As can be seen in Figure 3, the maximum temperature is bounded by the limiting cases for infinitely long and short cycle periods.

The relative invariance of the shape and the maximum of the temperature front can only be expected if the properties of the fixed bed are homogeneous and conversion is completed when the maximum temperature is reached. This is not the case with equilibrium-limited reactions since in this case conversion also takes place after the temperature maximum (Matros, 1986; Snyder and Subramaniam, 1993). A strong dependence of the maximum temperature on the cycle period can also be observed if the fixed bed is composed of portions with different properties. Figure 4 shows steady-state profiles in a reactor with inert front and end sections for different cycle periods. In this case, the maximum temperature varies significantly with the switching period. A discussion of this phenomenon has already been given in two earlier publications (Eigenberger and Nieken, 1988).

Stationary Traveling Wave as the Limiting Case for Long Switching Periods

We start from the balance equations of the two-phase model, Eqs. 1, 2, 3 and 4. First, the fixed axial coordinate z is transformed to the moving coordinate ξ, with $\xi = z - \omega t$, where ω is the moving velocity of a stationary moving front in an infinitely long fixed bed. After neglection of mass storage, axial thermal conduction and axial dispersion of mass in the fluid, the model equations for a single reaction are given as follows:

$$\omega \cdot (1-\epsilon) \cdot (\varrho c_p)_S \frac{dT^*}{d\xi} + (1-\epsilon) \cdot \lambda_S \cdot \frac{d^2T^*}{d\xi^2} + \alpha \cdot a_v \cdot (T - T^*) + (-\Delta hr) \cdot a_v \cdot r = 0 \quad (10)$$

$$\frac{\dot{m}}{A} \cdot c_{pG} \cdot \frac{dT}{d\xi} + \alpha \cdot a_v \cdot (T - T^*) = 0 \quad (11)$$

$$\frac{\dot{m}}{A} \cdot \frac{dg}{d\xi} + M_j \cdot a_v \cdot r = 0. \quad (12)$$

For an irreversible reaction the following boundary conditions can be specified:

$$T|_{\xi=-\infty} = T^*|_{\xi=-\infty} = T^0 \quad (13)$$

$$g|_{\xi=-\infty} = g^0 \quad (14)$$

$$T|_{\xi=+\infty} = T^*|_{\xi=+\infty} = T_{\max} \quad (15)$$

$$g|_{\xi=+\infty} = 0 \quad (16)$$

$$\left.\frac{dT}{d\xi}\right|_{z=\pm\infty} = \left.\frac{dT^*}{d\xi}\right|_{z=\pm\infty} = \left.\frac{dg}{d\xi}\right|_{z=\pm\infty} = 0. \quad (17)$$

Integration of Eqs. 10–12 from $\xi = -\infty$ to $\xi = +\infty$ using the preceding conditions, Eqs. 13–17 leads to the well-known relation between maximum temperature and velocity ω of the front (Wicke and Vortmeyer, 1959):

$$T_{\max} - T^0 = \frac{(\dot{m}/A) \cdot c_{pG} \cdot \Delta T_{ad}}{(\dot{m}/A) \cdot c_{pG} - (1-\epsilon) \cdot (\varrho c_p)_s \cdot \omega}. \quad (18)$$

Equations 10–18 can be solved to obtain the temperature and conversion profiles for a traveling reaction front. This is discussed in Appendix B. However, it turned out that a further modification leads to an easier solution.

If we insert Eqs. 11 and 12 into the energy balance for the solid phase, Eq. 10, and integrate along ξ over the whole temperature front, we obtain

$$(1-\epsilon) \cdot (\varrho c_p)_S \cdot \omega \cdot \int_{T^*}^{T_{\max}} dT^* + \lambda_S \cdot (1-\epsilon) \cdot \int_{dT^*/d\xi}^{0} d\left(\frac{dT^*}{d\xi}\right) - \frac{\dot{m}}{A} \cdot c_{pG} \cdot \int_{T}^{T_{\max}} dT - \frac{(-\Delta hr) \cdot \dot{m}}{M_j \cdot A} \cdot \int_{g}^{0} dg = 0. \quad (19)$$

Integration and elimination of the traveling velocity ω using Eq. 18 gives

$$(1-\epsilon) \cdot \lambda_S \frac{dT^*}{d\xi} = \frac{(-\Delta hr) \cdot \dot{m} \cdot g^0}{M_j \cdot A} \left(\frac{g}{g^0} - \frac{T_{\max} - T^*}{T_{\max} - T^0}\right) - \frac{\dot{m}}{A} \cdot c_{pG} \cdot (T^* - T). \quad (20)$$

A similar relation can be derived using the quasi-homogeneous energy balance Eq. 8 to yield

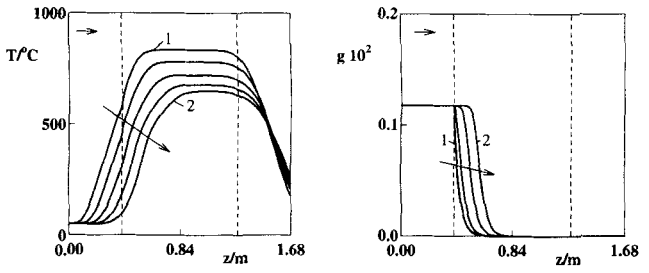

Figure 4. Influence of the switching period on (a) temperature profile and (b) reactant weight fraction profile in a reactor with inert front and end sections of 0.4 m each.

Plotted are the steady-state profiles with a switching period of 60 s (1), 90 s, 120 s, 150 s, and 180 s (2). (Parameter set 2, Table 1.)

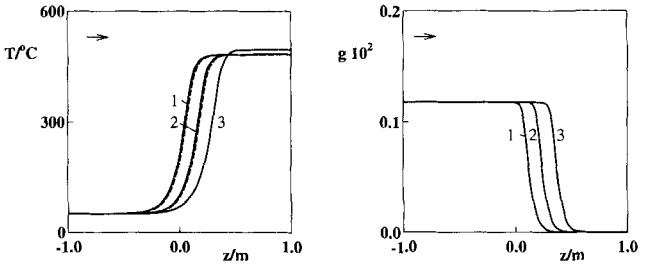

Figure 5. Calculation of the temperature and weight fraction in the moving reaction front.

(1) By discretization of the two-phase model, Eqs. 10–18 in space and solving the resulting system of nonlinear equations by Newton–Raphson; (2) by solving the two-phase model, Eqs. 11, 12, 20, as a boundary value problem in space as explained in Appendix B; (3) by using the quasi-homogeneous model described by Eqs. 12, 21. (Profiles are shifted for better comparison.)

$$\lambda_{\text{eff}}\frac{dT^*}{d\xi}=\frac{(-\Delta hr)\cdot\dot{m}\cdot g^0}{M_j\cdot A}\left(\frac{g}{g^0}-\frac{T_{\max}-T^*}{T_{\max}-T^0}\right). \quad (21)$$

Now Eqs. 11, 13, and 20 present a boundary-value problem with the unknown $T_{\max}$, which can be solved easily with the provisions given in Appendix B. Its solution gives the gas and solid temperature and the concentration profiles of the traveling reaction front. A further simplification is possible if the quasi-homogeneous model consisting of Eq. 12 and Eq. 21 is considered. A comparison of the solutions obtained from the different approaches discussed in this chapter is given for a specific example in Figure 5.

Approximation of the maximum temperature of the traveling wave

To find an approximation of the maximum temperature we follow the procedure proposed by Pinjala et al. (1988). Division of Eq. 12 by Eq. 21 renders

$$-\frac{(-\Delta hr)\cdot\dot{m}^2\cdot g^0}{M_j\cdot A^2\cdot\lambda_{\text{eff}}}\cdot\frac{dg}{dT^*}=\frac{M_j\cdot a_v\cdot r}{\dfrac{g}{g^0}-\dfrac{T_{\max}-T^*}{T_{\max}-T^0}}. \quad (22)$$

For a single reaction, where the rate expression can be written as an explicit function of the mass fraction g in the gas phase

$$r(g)=f(T^*,g)\cdot g \quad (23)$$

Eq. 22 becomes

$$-\frac{(-\Delta hr)\cdot\dot{m}^2}{M_j\cdot A^2\cdot\lambda_{\text{eff}}}\cdot\frac{dg}{dT^*}=\frac{M_j\cdot a_v\cdot f(T^*,g)}{1-\dfrac{T_{\max}-T^*}{T_{\max}-T^0}\cdot\dfrac{g^0}{g}}. \quad (24)$$

With the monotonicity of the temperature profile ($dT^*/d\xi \geq 0$) and assuming that $f(T^*, g)$ is monotonically increasing with g, the following inequality can be obtained [see Pinjala et al. (1988) and Nieken (1993) for details]:

$$\frac{(-\Delta hr)\cdot\dot{m}^2\cdot g^0}{M_j\cdot A^2\cdot\lambda_{\text{eff}}}>\int_{T^0}^{T_{\max}}M_j\cdot a_v\cdot f\left(T^*,\frac{T_{\max}-T^*}{T_{\max}-T^0}g_0\right)dT^*. \quad (25)$$

Equation 25 gives the general influence of all important parameters on $T_{\max}$ in a quasi-explicit form. If the Vortmeyer equivalence (Eq. 9) is used for λ_{eff}, Eq. 25 also includes the influence of the axial conduction in the solid and of the heat transfer between gas and packing separately. The mass-transfer resistance between gas and catalyst can be accounted for in the effective rate equation, Eq. 23. The only shortcoming is that Eq. 25 only gives an upper bound for $T_{\max}$ that may substantially exceed the true value, as we will see later (Figure 9).

The Countercurrent Reactor as the Limiting Case for Short Switching Periods

We have already mentioned that for rapid flow reversal the reverse-flow reactor approaches the state of a countercurrent reactor. To explain this limiting case the temperature profiles in a reversed-flow reactor are given in Figures 6a and 6b. If the direction of flow changes sufficiently rapidly, the solid temperature will not change—because of its large thermal capacity—while the gas temperature switches between the two profiles below or above the solid temperature on every flow reversal.

Instead of sending the mass flow $\dot{m}$ during one period in one direction and during the next period in the opposite direction, the same net result can be obtained by simultaneously sending half of it ($\dot{m}/2$) in each of the two directions (Figure 6c) and assuming that each of the two flows interacts with only one-half of the available catalyst. This means that the reactor and the catalyst are split into two halves with opposite flow directions: a countercurrent fixed-bed reactor arrangement results with heat exchange over a catalytic wall that is ideally permeable for heat but impermeable for mass.

If the two resulting compartments are given indices 1 and 2, respectively, the solid temperature profiles are identical, $T_1^* = T_2^* = T^*$, while the gas temperatures are mirror images of each other. Since $T^*(z)$ is a symmetric profile with zero

slope in the center, one can limit the considerations to one-half of the reactor.

The balance equations for the calculation of the steady-state behavior of the countercurrent reactor are given below. They refer to a countercurrent reactor in Figure 7.

Energy balance for catalyst:

$$0 = \lambda_S \cdot (1-\epsilon) \cdot \frac{d^2T^*}{dz^2} + \alpha \cdot \frac{a_v}{2} \cdot (T_1 - T^*) + \alpha \cdot \frac{a_v}{2} \cdot (T_2 - T^*) + \sum_{i=1}^{I} (-\Delta hr_i) \cdot \frac{a_v}{2} \cdot (r_{1i} + r_{2i}). \quad (26)$$

Energy balances for gas phases 1 and 2:

$$0 = -\frac{\dot{m}}{A} \cdot c_{pG} \cdot \frac{dT_1}{dz} + \lambda_{G,ax} \cdot \epsilon \cdot \frac{d^2T_1}{dz^2} - \alpha \cdot a_v \cdot (T_1 - T^*) \quad (27)$$

$$0 = \frac{\dot{m}}{A} \cdot c_{pG} \cdot \frac{dT_2}{dz} + \lambda_{G,ax} \cdot \epsilon \cdot \frac{d^2T_2}{dz^2} - \alpha \cdot a_v \cdot (T_2 - T^*) \quad (28)$$

Mass balances for gas phases 1 and 2:

$$0 = -\frac{\dot{m}}{A} \cdot \frac{dg_{1j}}{dz} + D_{\text{eff}} \cdot \epsilon \cdot \frac{d^2g_{1j}}{dz^2} - M_j \cdot \beta \cdot a_v \cdot (c_{1j} - c_{1j}^*) \quad (29)$$

$$0 = \frac{\dot{m}}{A} \cdot \frac{dg_{2j}}{dz} + D_{\text{eff}} \cdot \epsilon \cdot \frac{d^2g_{2j}}{dz^2} - M_j \cdot \beta \cdot a_v \cdot (c_{2j} - c_{2j}^*). \quad (30)$$

Mass balances for catalyst surfaces 1 and 2:

$$\beta_j \cdot a_v \cdot (c_{1j} - c_{1j}^*) = -a_v \cdot \sum_{i=1}^{I} \nu ij \cdot r_{1i} \quad (31)$$

$$\beta_j \cdot a_v \cdot (c_{2j} - c_{2j}^*) = -a_v \cdot \sum_{i=1}^{I} \nu ij \cdot r_{2i} \quad (32)$$

Boundary conditions:

$$\left.\frac{dT^*}{dz}\right|_{z=0} = 0 \qquad \left.\frac{dT^*}{dz}\right|_{z=L} = 0 \quad (33)$$

$$\left.\frac{dT_1}{dz}\right|_{z=0} = \frac{\dot{m} \cdot c_{pG}}{A \cdot \lambda_{G,ax} \cdot \epsilon} (T_1|_{z=0} - T_G^0) \qquad \left.\frac{dT_1}{dz}\right|_{z=L} = 0 \quad (34)$$

$$\left.\frac{dT_2}{dz}\right|_{z=0} = 0 \qquad \left.\frac{dT_2}{dz}\right|_{z=L} = \frac{-\dot{m} \cdot c_{pG}}{A \cdot \lambda_{G,ax} \cdot \epsilon} (T_2|_{z=L} - T_G^0) \quad (35)$$

$$\left.\frac{dg_{1j}}{dz}\right|_{z=0} = \frac{\dot{m}}{A \cdot D_{\text{eff}} \cdot \epsilon} \left(g_{1j}|_{z=0} - g_j^0\right) \qquad \left.\frac{dg_{1j}}{dz}\right|_{z=L} = 0 \quad (36)$$

$$\left.\frac{dg_{2j}}{dz}\right|_{z=0} = 0 \qquad \left.\frac{dg_{2j}}{dz}\right|_{z=L} = \frac{-\dot{m}}{A \cdot D_{\text{eff}} \cdot \epsilon} \left(g_{2j}|_{z=L} - g_j^0\right). \quad (37)$$

The solution of the preceding two-point boundary-value problem requires spatial discretization and iterative solution of the resulting system of nonlinear equations.

Quasi-homogeneous model of the countercurrent reactor

Using an approximation outlined in Appendix A, the three energy balances (Eqs. 26–28) can be lumped into a single quasi-homogeneous energy balance:

$$\lambda_{\text{eff}} \cdot \frac{d^2T^*}{dz^2} + \sum_{i=1}^{I} (-\Delta hr_i) \cdot \frac{a_v}{2} \cdot (r_{1i} + r_{2i}) = 0 \quad (38)$$

with

$$\lambda_{\text{eff}} = \lambda_S \cdot (1-\epsilon) + \left(\frac{\dot{m} \cdot c_{pG}}{A}\right)^2 \cdot \frac{1}{\alpha \cdot a_v}. \quad (39)$$

Now the resulting energy balance, Eq. 38, is elliptic, which allows the use of shooting methods for the numerical solution. Using a different approach, Matros (1989) derived equations for the so-called "sliding regime," which are equivalent to the preceding equations for the countercurrent reactor.

Considering only one reaction and neglecting axial dispersion in both gas phases, the mass balances, Eqs. 29–32, can again be inserted into the energy balance of the quasi-homogeneous model, Eq. 38. Assuming constant physical properties, the energy balance obtained can be integrated once. The resulting system then consists of three ordinary differential equations:

$$0 = \lambda_{\text{eff}} \cdot \frac{dT^*}{dz} + \frac{(-\Delta hr) \cdot \dot{m}}{2 \cdot M_j \cdot A} \cdot (g_2 - g_1) \quad (40)$$

$$0 = \frac{\dot{m}}{A} \cdot \frac{dg_1}{dz} + M_j \cdot a_v \cdot r_1 \quad (41)$$

$$0 = \frac{\dot{m}}{A} \cdot \frac{dg_2}{dz} - M_j \cdot a_v \cdot r_2. \quad (42)$$

The following boundary conditions apply (see Appendix A):

Reactor inlet:
$$T|_{z=0}^* = T^0 + \frac{\Delta T_{ad}}{2} \cdot \left(1 - \frac{g^e}{g^0}\right) \quad (43)$$

$$g_1|_{z=0} = g^0 \quad (44)$$

$$g_2|_{z=0} = g^e. \quad (45)$$

Since at the middle of the reactor ($z = L/2$) the conditions must be identical in both channels 1 and 2,

$$g_1|_{z=L/2} = g_2|_{z=L/2}. \quad (46)$$

Equations 40–46 specify a two-point boundary-value problem where either the outlet concentration g^e or the length of the reactor is unknown.

By integrating Eqs. 40–42 with a given outlet concentration, temperature and concentration profiles of the countercurrent reactor can be calculated directly. We will use this technique later to compute all three steady states of the countercurrent reactor in the region of steady-state multiplicity. The method can be extended to also treat multiple reactions.

Simple approximation of the reactor profiles

If a first-order reaction is assumed and full conversion is reached in the middle of the reactor, the maximum temperature can easily be computed directly from the preceding model.

The reaction rate shall be given as

$$r_1 = B(T^*) \cdot g_1, \tag{47}$$

where $B(T^*)$ includes the Arrhenius dependency of the rate constant and allows for the consideration of a mass-transfer resistance between the flowing gas and the catalyst surface. Dividing Eq. 41 by Eq. 40 leads to

$$\frac{\dot{m}}{A \cdot \lambda_{\text{eff}}} \cdot \frac{dg_1}{dT^*} = \frac{2 \cdot a_v \cdot M_j^2 \cdot A}{(-\Delta hr) \cdot \dot{m}} \cdot \frac{r_1}{g_2 - g_1} \tag{48}$$

where $g_2 = 0$ for $0 \le z \le L/2$, if full conversion before the middle of the reactor is assumed. Separation of variables and integration from $z = 0$ to $z = L/2$ gives

$$\frac{(-\Delta hr) \cdot \dot{m}^2 \cdot g^0}{2 \cdot M_j \cdot A^2 \cdot \lambda_{\text{eff}}} = \int_{T^0 + \Delta T_{ad}/2}^{T_{\max}} M_j \cdot a_v \cdot B(T^*)\, dT^*. \tag{49}$$

Through evaluation of the integral on the righthand side, the maximum temperature can be obtained. Equation 49 for the countercurrent reactor is similar to Eq. 25 for the traveling wave except for a factor of 2 in the denominator of the left-hand side and the inequality sign. Contrary to Eq. 25, only well-justified assumptions had to be used for its derivation.

As an example, the case of a mass-transfer-limited first-order reaction is considered in more detail: Assuming $r = -k(T^*) \cdot c^*$ and using $c = (\varrho_G / M_L) \cdot g$, one obtains from Eq. 31.

$$c^* = \frac{\beta}{\beta + k(T^*)} c,$$

hence

$$r = k(T^*) c^* = \frac{\beta k(T^*) \varrho_G}{M_j (\beta + k(T^*))} g. \tag{50}$$

Rewriting Eq. 49 by using the residence time, τ, the adiabatic temperature rise ΔT_{ad}, and the Peclet number, Pe, to characterize the relation of convective to conductive energy transport gives

$$\underbrace{\frac{c_{pG} \cdot \dot{m}/A \cdot L}{\lambda_{\text{eff}}}}_{Pe} \cdot \frac{\Delta T_{ad}}{2} \cdot \underbrace{\frac{\dot{V}}{V_R}}_{1/\tau} = \int_{T^0 + \Delta T_{ad}/2}^{T_{\max}} a_v \cdot \frac{\varrho(T^*)}{\varrho(T^0)} \cdot \frac{k(T^*) \cdot \beta}{k(T^*) + \beta} dT^*. \tag{51}$$

From this equation the influence of all relevant parameters on the maximum temperature can be obtained.

As we have seen from Figure 3 the temperature gradient in the reaction front of the reversed-flow reactor can be approximated by the temperature gradient of the countercurrent reactor at $z = 0$. The latter can be calculated from Eq. 40 with $g_2 = 0$, giving

$$\left.\frac{dT^*}{dz}\right|_{z=0} = \frac{\Delta T_{ad} \cdot \dot{m} \cdot c_{pG}}{2 \cdot \lambda_{\text{eff}} \cdot A}. \tag{52}$$

With the maximum temperature from Eq. 49 or Eq. 51, the velocity of the moving thermal front can be approximated by Eq. 18:

$$\omega = \frac{\dot{m}/A \cdot c_{pG}}{(1-\epsilon) \cdot (\varrho c_p)_S} \cdot \left(1 - \frac{\Delta T_{ad}}{T_{\max} - T^0}\right). \tag{53}$$

Given the length of a switching period, one can then calculate the front displacement within one period.

Equations 51 to 53 give a concise description of all relevant features of both a reverse-flow or a countercurrent fixed-bed reactor. Examples can be found in Eigenberger and Nieken (1991), Nieken (1993), and Nieken et al. (1994). Figure 8 compares temperature profiles constructed from these equations with the steady-state temperature profiles for the reverse-flow reactor calculated with the full two-phase model. The good agreement proves that the approximate solutions can be used as reasonable initial guesses for the calculation of the steady state of a reverse-flow reactor. Figure 9 shows the differences in maximum temperatures obtained with the upper limit estimate of Pinjala et al. (1988), Eq. 25, with the quasi-homogeneous model for a traveling wave, Eqs. 12 and 21, and with the countercurrent reactor model, Eqs. 40–42, for the case of a monolith catalyst with differing solid heat conductivity λ_S or channel diameter d_h (see Nieken, 1993 for details). It can be seen that Eq. 25 overestimates $T_{\max}$ but predicts the tendency qualitatively correct.

Multiple Steady States in the Countercurrent Reactor

Autothermal operation is usually carried out in the region of multiple steady states where the ignited steady state is the desired one. Under reversed-flow operation one single steady state will only exist if

- The inlet temperature is low and the heat evolution and recovery is too small to sustain the ignited state, or
- The inlet temperature is high enough and/or the reactor is long enough for full conversion to occur even if there is no flow reversal and heat recovery.

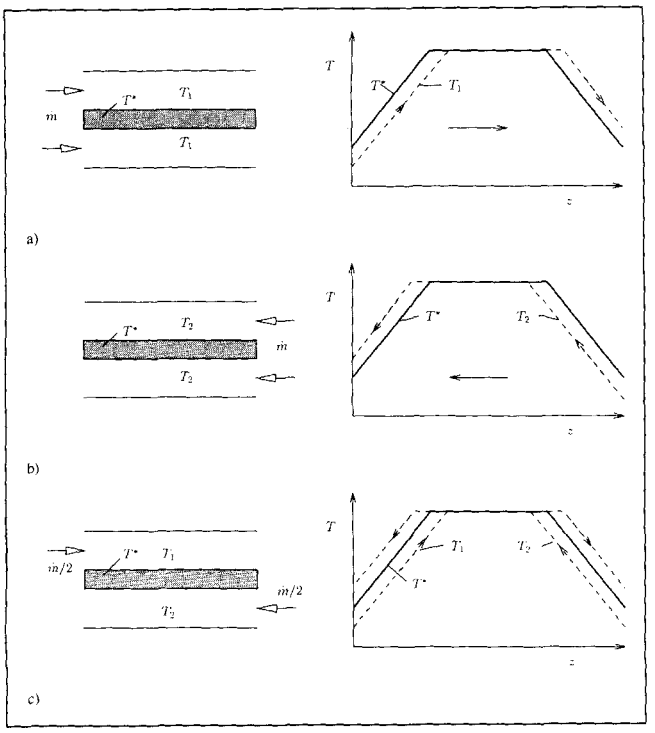

Figure 6. Reactor with simplified temperature profiles for rapid flow reversal ((a) and (b)) and a countercurrent fixed-bed reactor ((c)).

Temperature in the solid phase (——), temperature in the gas phase (– –).

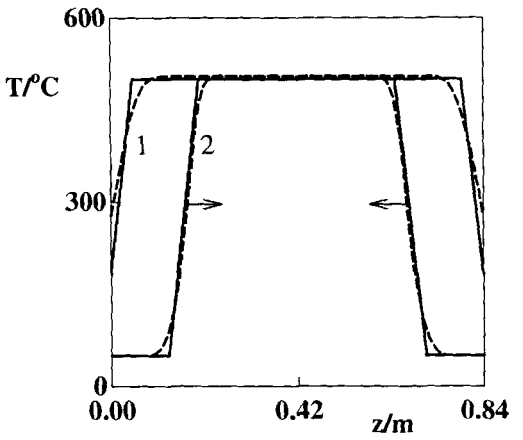

Figure 8. Solid lines show the temperature profiles constructed from the maximum temperature, Eq. 51, and the initial slope, Eq. 52, of the countercurrent reactor.

The front displacement from 1 to 2 was calculated using Eq. 53 and the switching period. The dotted lines show the temperature profiles calculated with the two-phase model at the times of the flow reversal. (Parameters set 1, Table 1.)

By dynamic simulation only the stable steady states can be computed. The unstable steady state, which separates the ignited and the extinguished solution, is of interest for the start up of the reactor, because only a temperature profile higher than the profile of the unstable steady state leads to ignition. If two or more components are to be oxidized, up to five steady states can be found, three of them being stable and separated by two unstable solutions. This subject has been addressed elsewhere (Nieken et al., 1994).

Here only a single first-order reaction is considered. Using the model with quasi-homogeneous energy balance, one can compute temperature and concentration profiles by specifying the length of the reactor and integrating the initial-value problem, Eqs. 40–42, from $z = 0$ to $z = L$ for a given value of g^e and improve g^e iteratively until the closure condition, Eq. 46, is fulfilled. To calculate all possible steady states we go the opposite way. First a specific conversion U is chosen that determines the outlet concentration g^e. Then one has to find the reactor length that satisfies the symmetry condition, Eq. 46.

Figure 10 shows the reactor length z as a function of the conversion U. In a sufficiently long reactor only the ignited state exists; in a very short reactor only the extinguished state exists. In between, three steady states are obtained. The temperature and concentration profiles of the unstable and the ignited solution at a moderate reactor length are shown in Figure 11. The extinguished solution near $T^*(z) = T^0$, $g(z) = g^0$ is not plotted.

Figure 12 shows the maximum temperature and the conversion as a function of the reactor length. The parameter is the feed concentration given as the adiabatic temperature rise. In Figure 13 the maximum temperature is plotted over the adiabatic temperature rise for a given reactor length. In the case of the monolith reactor considered, the conversion remains close to 100% as the inlet concentration is lowered to the point where extinction occurs, while the maximum temperature decreases almost linearly with decreasing feed concentration (ΔT_{ad}).

Conclusions

For most parametric studies only the cyclic steady-state solution of the reverse-flow reactor is of interest. Its calculation by solving the model equations over a large number of cycle periods requires a considerable computational effort. If the fixed bed has constant physical properties and only irreversible reactions take place, the maximum temperature and

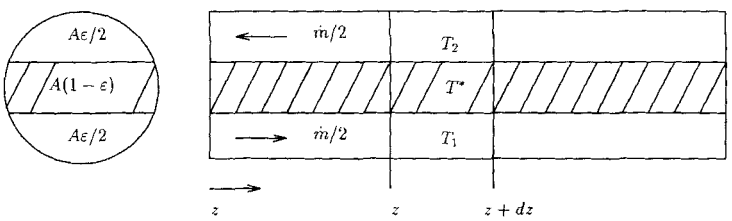

Figure 7. Countercurrent reactor for the derivation of the balance equations (Eqs. 26–37).

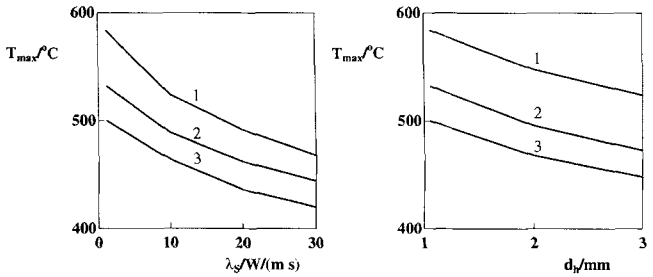

Figure 9. Maximum temperature as a function of solid heat conductivity λ_S and hydraulic channel diameter d_h for a monolith fixed bed.

(1) Calculated with the traveling wave approximation of Pinjala et al., Eq. 25; (2) calculated with the quasi-homogeneous model for a traveling wave, Eqs. 12, 21; (3) with the countercurrent reactor model Eqs. 40–42.

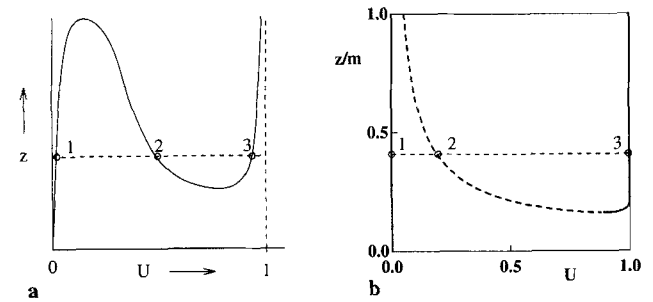

Figure 10. Conversion U in the quasi-homogeneous countercurrent reactor as a function of the rector length z.

Solutions 1 and 3 are stable. (a) General behavior; (b) oxidation of propane. (Parameter set 1, Table 1).

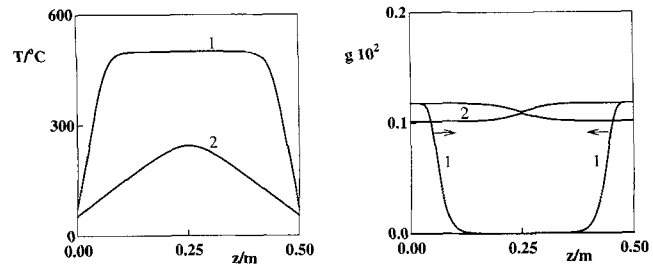

Figure 11. Steady-state temperature and concentration profiles in a countercurrent reactor.

(1) Upper stable solution; (2) unstable solution. (Parameters set 1, Table 1).

the slope of the temperature front is almost invariant to the cycle period. Therefore, it is sufficient to calculate the limiting cases of very long or very short cycle periods. In the latter case, the reactor approaches the state of a countercurrent reactor; in the first case, a stationary traveling wave is formed. By using the integrated form of the quasi-homogeneous energy balance, Eq. 21 or 40, both cases can be calculated rapidly.

If, for a single reaction, the kinetics can be split into a temperature-dependent term and a term depending linearly on the gas concentration, the maximum temperature can be calculated from a single equation, Eq. 49 or 51. From this

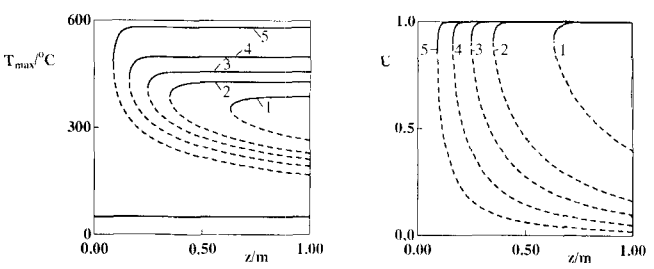

Figure 12. Maximum temperature T_{max} and conversion U for different feed concentrations as a function of the reactor length.

(1) ΔT_{ad} = 10 K; (2) ΔT_{ad} = 20 K; (3) ΔT_{ad} = 30 K; (4) ΔT_{ad} = 50 K; (5) ΔT_{ad} = 100 K. (Parameter set 1, Table 1).

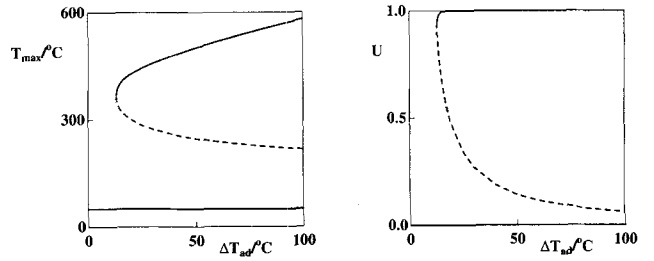

Figure 13. Maximum temperature T_{max} and conversion U as a function of the feed concentration, given as adiabatic temperature rise of the feed.

(Reactor length: L = 0.5 m, parameter set 1, Table 1.)

equation the influence of all model parameters on the maximum temperature can be determined. If the maximum temperature is known, the slope and the traveling velocity of the reaction front can be obtained directly from Eqs. 52 and 53. Maximum temperature, slope, and traveling velocity allow for an approximate construction of the steady-state temperature profile.

For the limiting case of the countercurrent reactor the unstable solution between the ignited and the extinguished steady state can also be calculated. This is important for process control since it is the lowest temperature profile from which the reaction can ignite.

Acknowledgment

The work reported here was supported by the Ministry of the Federal Republic of Germany, grant no. 0326902A.

Notation

a_v = specific surface area, m^2/m^3
A = cross-sectional area of reactor, m^2
c_p = specific heat capacity, kJ/(kg·K)
D_{eff} = effective mass-dispersion coefficient, kg/(m·s)
E = activation energy, kJ/kmol
G_z = specific mass-flow rate, kg/(m^2·s)
Δh_{ri} = enthalpy of reaction i, kJ/kmol
k = rate constant, m/s
L = length of catalyst bed, m
M_L = molecular weight of air, kg/kmol

Nu = Nusselt number
p = pressure, Pa
r = reaction rate, related to the outer surface of the catalyst, $kmol_i/(m^2 \cdot s)$
Sh = Sherwood number
t = time, s
V_R = volume of the reactor, m^3
α = heat-transfer coefficient, $W/(m^2 \cdot K)$
β = mass-transfer coefficient, m/s
ϵ = void fraction
ϱ = density, kg/m^3

Subscripts and Superscript

i = reaction index ($i = 1 \ldots I$)
L = air
1 = flow from left to right
2 = flow from right to left
0 = feed

Literature Cited

Bhatia, S. K., "Analysis of Catalytic Reactor Operation with Periodic Flow Reversal," *Chem. Eng. Sci.*, **46**(1), 361 (1991).

Boreskov, G. K., O. V. Kiselev, and Y. S. Matros, "Catalytic Processes Carried Out Under Nonstationary Conditions: Thermal Front in a Fixed Bed of Catalyst," *Kinet. Katal.*, **20**(3), 773 (1979).

Boreskov, G. K., and Y. S. Matros, "Unsteady-State Performance of Heterogeneous Catalytic Reactions," *Catal. Rev.-Sci. Eng.*, **25**(4), 551 (1983).

Boreskov, G. K., Y. S. Matros, G. A. Bunimovich, and A. A. Ivanov, "Catalytic Processes Carried Out Under Non-Steady-State Conditions: Switching the Direction for the Feed of the Reaction Mixture to the Catalyst Bed. Experimental Results," *Kinet. Katal.*, **23**(2), 402 (1982).

Chen, Y. C., and D. Luss, "Wrong-Way Behavior of Packed-Bed Reactors: Influence of Interphase Transport," *AIChE J.*, **35**(7), 1148 (1989).

Chumakova, N. A., and Y. S. Matros, "Isolating Laminar-Flow Regimes with Periodic Sweep Reversal in a Fixed Catalyst Layer," *Teor. Osn. Khim. Tekhnol.*, **25**(3), 369 (1991).

Dankwerts, P. V., "Continuous Flow Systems," *Chem. Eng. Sci.*, **2**, 1 (1953).

Deuflhard, P., "Numerik von Anfangswertproblemen für gewöhnliche Differentialgleichungen," *TR 89-2, Konrad-Zuse-Zentrum für Informationstechnik Berlin*, Berlin, Germany (1989).

Eigenberger, G., and U. Nieken, "Catalytic Combustion with Periodic Flow Reversal," *Chem. Eng. Sci.*, **42**, 2109 (1988).

Eigenberger, G., and U. Nieken, "Katalytische Abluftreinigung: Verfahrenstechnische Aufgaben und neue Lösungen," *Chem. Ing. Tech.*, **63**(8), 781 (1991). (English version published in *Int. J. Chem. Eng.*, **34**, 4 (1994).)

Epple, U., *Ein reduziertes Modell zur Beschreibung von Wellenausbreitungsvorgängen in nichtlinearen verteilten Systemen*, Diss., Univ. Stuttgart, Stuttgart, Germany (1986).

Gilles, E. D., "Quasi-stationäres Verhalten von wandernden Brennzonen," *Chem. Eng. Sci.*, **29**, 1211 (1974).

Gupta, V. K., and S. K. Bhatia, "Solution of Cyclic Profiles in Catalytic Reactor Operation with Periodic Flow Reversal," *Comput. Chem. Eng.*, **15**(4), 229 (1991).

Kiselev, O. V., and Y. S. Matros, "Propagation of the Combustion Front of a Gas Mixture in a Granular Bed of Catalyst," *Combustion, Explos. Shock Waves*, **16**, 152 (1980).

Matros, Y. S., "Unsteady-State Oxidation of Sulphur Dioxide for Sulphuric Acid Production," *Sulphur*, **183**, 23 (1986).

Matros, Y. S., *Catalytic Processes Under Unsteady-State Conditions*, Elsevier, Amsterdam (1989).

Matros, Y. S., A. S. Noskow, V. A. Chumachenko, and O. V. Goldman, "Theory and Application of Unsteady Catalytic Detoxication of Effluent Gases from Sulphur Dioxide, Nitrogen Oxides and Organic Compounds," *Chem. Eng. Sci.*, **43**(8), 2061 (1988).

Matros, Y. S., A. S. Noskov and V. A. Chumachenko, "Progress in Reverse-Process Application to Catalytic Incineration Problems," *Chem. Eng. Process.*, **32**, 89 (1993).

Nieken, U., *Abluftreinigung in katalytischen Festbettreaktoren bei periodischer Strömungsumkehr*, VDI-Verlag, Düsseldorf (1993).

Nieken, U., G. Kolios, and G. Eigenberger, "Fixed Bed Reactors with Periodic Flow Reversal: Experimental Results for Catalytic Combustion," *Cat. Today*, **99**(20), 335 (1995).

Nowak, U., J. Frauhammer, U. Nieken, and G. Eigenberger, "A Fully Adaptive Algorithm for Parabolic Partial Differential Equations in One Space Dimension," *Comp. Chem. Eng.*, in press (1995).

Pinjala, V., Y. C. Chen, and D. Luss, "Wrong-Way Behavior of Packed-Bed Reactors: II. Impact of Thermal Dispersion," *AIChE J.*, **34**(10), 1663 (1988).

Schlünder, E. U., "Equivalence of One and Two-Phase Models for Heat Transfer Processes in Packed Beds: One Dimensional Theory," *Chem. Eng. Sci.* (Letters to the Editors), **30**, 449 (1975).

Snyder, J. D., and B. Subramaniam, "Numerical Simulation of a Periodic Flow Reversal Reactor for Sulfur Dioxide Oxidation," *Chem. Eng. Sci.*, **48**(24), 4051 (1993).

Vortmeyer, D., and R. J. Schäfer, "Equivalence of One and Two-Phase Models for Heat Transfer Processes in Packed Beds: One Dimensional Theorie," *Chem. Eng. Sci.*, **29**, 485 (1974).

Wicke, E., and D. Vortmeyer, "Zündzonen heterogener Reaktionen in gasdurchströmten Körnerschichten," *Ber. Bunsenges.*, **63**, 145 (1959).

Appendix A: Quasi-homogeneous Model for the Countercurrent Reactor

If the heat conduction in the gas phase ($\lambda_{G,ax}$) is negligible compared to the conduction in the solid phase (λ_S), the three energy balance equations, Eqs. 26–28 can be added to yield

$$2(1-\epsilon)\lambda_S \frac{d^2T^*}{dz^2} + \sum_{i=1}^{I} (-\Delta h_{ri}) a_v (r_{1i} + r_{2i}) + \frac{\dot{m}}{A} c_{pG} \left(\frac{dT_2}{dz} - \frac{dT_1}{dz} \right) = 0. \quad \text{(A1)}$$

After differentiation and subtraction, Eqs. 27 and 28 give

$$\frac{\dot{m}}{A} c_{pG} \left(\frac{d^2T_1}{dz^2} + \frac{d^2T_2}{dz^2} \right) = \alpha a_v \left(\frac{dT_2}{dz} - \frac{dT_1}{dz} \right). \quad \text{(A2)}$$

From Figure 6c it can be concluded that $T^* = (T_1 + T_2)/2$ is a reasonable approximation for the important part of the temperature profile where heat exchange between compartments 1 and 2 without chemical reaction dominates. Inserted into Eq. A2 and combined with Eq. A1, the energy balance of the quasi-homogeneous model, Eq. 38 is obtained:

$$\underbrace{\left\{ (1-\epsilon)\lambda_S + \frac{1}{\alpha a_v} \left(\frac{\dot{m}}{A} c_{pG} \right)^2 \right\}}_{\lambda_{\text{eff}}} \frac{d^2T^*}{dz^2} + \frac{a_v}{2} \sum_{i=1}^{I} (-\Delta h_R)_i (r_{1i} + r_{2i}) = 0.$$

It is interesting to note that the resulting effective thermal conductivity λ_{eff} is identical to that of the Vortmeyer equivalence relation, Eq. 9. This relation had been criticized occasionally because of its apparently empirical nature (Schlünder, 1975), but it has proved to be a very reliable approximation in practice.

In the case of one reacting component, the quasi-homogeneous energy balance can be further reduced to Eq. 40, as discussed in the section titled "The quasi-homogeneous model of the countercurrent reactor." From an overall energy balance over the adiabatic countercurrent reactor, it is obvious that

$$T_2|_{z=0} = T_1|_{z=0} + \Delta T_{ad}\left(\frac{g^0 - g^e}{g^0}\right).$$

With $T|_{z=0} = T^* = (T_1|_{z=0} + T_2|_{z=0})/2$ and $T_1|_{z=0} = T^0$, the boundary condition, Eq. 43, is obtained.

Appendix B: Numerical Solution of the Traveling Reaction Front Problem

Our first attempts to use shooting methods for the solution of the system of Eqs. 10–18 failed because the related initial-value problem is ill-conditioned (Deuflhard, 1989). One possible way to solve the boundary-value problem is spatial discretization of Eq. 10 to Eq. 18 and the iterative solution of the resulting system. If a Newton–Raphson iteration is applied, the initial guesses of the temperature profile and of the moving velocity have to be quite accurate to obtain convergence.

A much easier way turned out to be the following: Eq. 20 together with Eqs. 11 and 12 represent an initial-value problem for $g(\xi)$, $T^*(\xi)$, and $T(\xi)$, which contains the unknown variable T_{max}. To calculate the temperature and concentration profiles, an appropriate starting point $\xi = 0$ has to be chosen. A good choice is a point of the traveling front where $T^*_{\xi=0}$ is a few degrees greater than T^0, but smaller than the temperature above which any noticeable reaction takes place. Therefore, the initial conditions are $g|_{\xi=0} = g^0$; $T^*_{\xi=0} = T^0 + \delta$. An additional difficulty is the determination of consistent values for the initial temperatures of the gas and solid phases. These values can be found in the following way: For a given bed temperature $T^*_{\xi=0}$, assuming no conversion for $\xi < 0$, the gas temperature $T_{\xi=0}$ can be calculated analytically by solving the two energy balances between $-\infty < \xi < 0$, with $T_{\xi=-\infty} = T^*_{\xi=-\infty} = T^0$. The method presented can also be used for more than one reactive component (see Nieken, 1993, for details).

To obtain T_{max} one can start with an initial guess and integrate the three equations along the axial coordinate with any method for nonstiff ordinary differential equations. If the initial guess for T_{max} is too high, the calculated temperature profiles will have a relative maximum and drift to $-\infty$ for large values of ξ. In the opposite case the temperature will rise to $+\infty$. By using, for example, the Regula–Falsi method, the iteration procedure will converge rapidly, yielding the correct solution profiles for $T^*(\xi)$, $T(\xi)$, and $g(\xi)$.

The same kind of procedure can be applied for the quasi-homogeneous model, Eqs. 12 and 21 as well.

Manuscript received Jan. 18, 1994, and revision received Sept. 28, 1994.